Stability of liquid channels or filaments in the presence of line tension

2005 J. Phys.: Condens. Matter 17 2349

(http://iopscience.iop.org/0953-8984/17/15/008)

INSTITUTE OF PHYSICS PUBLISHING JOURNAL OF PHYSICS: CONDENSED MATTER

J. Phys.: Condens. Matter **17** (2005) 2349–2364 doi:10.1088/0953-8984/17/15/008

Stability of liquid channels or filaments in the presence of line tension

Martin Brinkmann[1,2], **Jan Kierfeld**[1] **and Reinhard Lipowsky**[1]

[1] MPI für Kolloid-und Grenzflächenforschung, D-14424 Potsdam, Germany[3]
[2] Interdisciplinary Research Institute, c/o IEMN, F-59652 Villeneuve d'Ascq, France

Received 22 November 2004, in final form 25 February 2005
Published 1 April 2005
Online at stacks.iop.org/JPhysCM/17/2349

Abstract

The local stability of a cylindrical liquid channel or filament deposited on a planar homogeneous substrate is studied in the framework of an effective interface model including the line tension of the three phase contact line. We discuss the stability with respect to transversally symmetric and antisymmetric deformation modes and compute a stability diagram in terms of the contact angle and the longitudinal wavelength of these modes for different values of line tension. An increase in the line tension always leads to an increase in the local stability of liquid channels or filaments. For large positive line tension, the behaviour with pinned contact lines is recovered. As one decreases the line tension to negative values, deformation modes of arbitrary wavelength destabilize the channel or filament for sufficiently small contact angles. In addition, a negative line tension leads to a band of unstable short wavelength modes within the continuum theory considered here. It is argued that the presence or absence of these latter modes depends on the ratio of the contact line width to the molecular size.

(Some figures in this article are in colour only in the electronic version)

[3] http://www.mpikg-golm.mpg.de/th/

List of symbols

α	Vapour or low density phase
β	Wetting liquid or high density phase
θ	Local contact angle of droplet
Λ	Line tension of three phase contact line
$\bar{\Lambda}$	Rescaled line tension $\bar{\Lambda} \equiv \Lambda / \Sigma_{\alpha\beta} L_\perp$
λ	Longitudinal wavelength
$\bar{\lambda}$	Rescaled wavelength $\bar{\lambda} \equiv \lambda / L_\perp$
μ	Eigenvalue of second variation of free energy
$\bar{\mu}$	Rescaled eigenvalue $\bar{\mu} \equiv \mu L_\perp^2$
$\mu_\perp$	Transverse part of eigenvalue
Σ_{ij}	Surface tension of interface between phases i and j
σ	Rigid and inert substrate
φ	Azimuthal angle on the cylinder segment
$\mathscr{A}_{\alpha\beta}$	Interface between fluid α and liquid β
$k_\parallel$	Longitudinal wavenumber
$k_\perp$	Transverse wavenumber
$\mathscr{L}_{\alpha\beta\sigma}$	Three phase contact line
$L_\parallel$	Channel length
$L_\perp$	Channel width
x	Rescaled wavenumber $x \equiv k_\perp \theta$
z	Coordinate parallel to the axis of the cylinder

1. Introduction

Wetting morphologies of small liquid droplets have received a lot of experimental and theoretical interest in recent years [1]. Novel AFM imaging techniques made it possible to study the morphology of tiny droplets wetting a solid substrate for droplet sizes down to the nanometre regime [2]. It is experimentally and theoretically well established that a change in the droplet volume can trigger morphological instabilities such as the bulging of a liquid channel or filament adsorbed onto a lyophilic stripe [3, 4].

The stability of small wetting structures can be theoretically studied by minimizing their free energy which contains interfacial contributions from the liquid–vapour interface and the substrate surface, and line tension contributions from the three phase contact line. The minimization can be performed analytically for sufficiently simple wetting morphologies such as, for example, liquid droplets with spherical liquid–vapour interfaces in contact with the inner surface of a cone [5]. Even in this simple wetting geometry a rich polymorphism of equilibrium droplet shapes emerges which is controlled by line tension, wettability, and cone angle.

The line free energy becomes increasingly important for the stability of the wetting structure with decreasing droplet size. We expect that line tension effects cannot be ignored on length scales below about one hundred nanometres [1, 6]. The line tension can assume positive or negative values depending on the particular form of the molecular interactions [6, 7]. Therefore, we will explore the effects of both positive and negative line tensions on the stability of small wetting structures.

In [8], we have derived a general stability criterion which allows us to systematically study the stability of wetting morphologies, including line tension. This stability criterion is now employed to investigate the stability of a cylindrical liquid channel or filament for arbitrary contact angle on a homogeneous substrate. The geometry of a liquid channel is of relevance not only because it represents one of the most basic wetting morphologies used in microfluidic devices. It is also of more general theoretical interest as it is closely related to another well-known interfacial instability: the breakup of a free-standing liquid cylinder into disconnected droplets caused by long wavelength shape perturbations, first described by Rayleigh and Plateau [11]. A similar instability occurs for liquid channels or filaments wetting a homogeneous substrate: for contact angle $\theta = \pi/2$, the latter instability occurs, by symmetry, at the unstable wavelength of the full cylinder [12, 13]. In the present paper, we study how positive or negative line tension affects the stability of such wetting morphologies of the three phase contact line.

We first present a systematic analysis of the stability against different deformation modes based on the stability criterion derived in [8]; see also [9, 10]. This leads to a complete stability diagram of a liquid channel in contact with a homogeneous substrate in terms of the contact angle θ, the longitudinal wavelength λ of the shape perturbations imposed onto the liquid structure, and the line tension Λ; see figure 4 below.

Positive line tensions have a stabilizing effect and tend to suppress the Rayleigh–Plateau-like instability. Any small positive line tension represents a perturbation which stabilizes the channel against deformation modes up to a longitudinal wavelength $\lambda \propto 1/\theta$ for small θ. For contact angles $\theta > \pi/2$, on the other hand, we show that there always remains a region of instability at sufficiently long wavelengths. In the limit of large positive line tension, this becomes identical with the instability region for pinned contact lines as determined in [3, 13].

As one decreases the line tension towards negative values, all deformation modes become unstable for sufficiently small contact angles $\theta < \theta_{\min}$ with $\theta_{\min} \approx c_{\min}\sqrt{|\bar{\Lambda}|}$ and $c_{\min} \simeq 2.90$ for small negative line tension Λ. In addition, a negative line tension leads to a band of unstable short wavelength modes within the continuum theory considered here. Dimensional analysis shows that the presence or absence of these latter modes depends on the ratio c_Λ of the intrinsic width of the contact line to the molecular size within the liquid phase: these short wavelength modes should be absent and present if $c_\Lambda \simeq 1$ and $c_\Lambda \gg 1$, respectively.

This paper is organized as follows. Section 2 contains a brief outline of the equilibrium conditions and the general stability criterion that govern the morphological behaviour of droplets wetting rigid substrates in the presence of line tension. This stability criterion is applied to the particular droplet geometry of a cylindrical liquid channel or filament in the following section 3. A transcendental equation in a transverse wavenumber of symmetric and antisymmetric deformation modes is numerically solved and discussed for the case of vanishing line tension in section 4. In the subsequent section 5 we then describe the impact of a positive and negative line tension on the stability of the liquid channel or filament as illustrated in the form of a stability diagram and compute the asymptotic scaling forms of the stability limits.

2. Equilibrium conditions and droplet stability

Let us consider a droplet of an incompressible liquid β in contact with the surface of a chemically inert and rigid substrate σ. The ambient fluid α may be a vapour phase or another liquid immiscible with β. Provided that the vertical extension of the droplet is significantly smaller than the capillary length one can regard the $\alpha\beta$ interface at mechanical equilibrium

as a surface of constant mean curvature [1]. The mean or extrinsic curvature M of the $\alpha\beta$ interface is defined as the sum $M = (c_1 + c_2)/2$ of local principal curvatures c_1 and c_2 (for a definition of the principal curvatures see, for instance, do Camo [14]). For later convenience we will use the symbol $\mathscr{A}_{\alpha\beta}$ for the mathematical surface that describes the $\alpha\beta$ interface of a droplet, and in the particular case considered here, that of a liquid channel.

The condition of mechanical equilibrium between the $\alpha\beta$ interface and the adjacent fluid phases α and β is given by the Laplace equation

$$2\Sigma_{\alpha\beta}M = P_\beta - P_\alpha \qquad \text{on } \mathscr{A}_{\alpha\beta}, \tag{1}$$

which relates the surface tension $\Sigma_{\alpha\beta}$ and the mean curvature M of the $\alpha\beta$ interface to the local difference in bulk pressure P_i between the fluids $i = \alpha, \beta$ [1]. If the influence of gravity is negligible the bulk pressures can be considered as position independent which, provided that the surface tension $\Sigma_{\alpha\beta}$ is the same in each point on the $\alpha\beta$ interface, implies a constant mean curvature M.

A second, independent condition of mechanical equilibrium is related to the $\alpha\beta\sigma$ line where the substrate σ and the fluid phases α and β meet. Since the system under consideration comprises only three phases, we will simply refer to the $\alpha\beta\sigma$ line as the contact line of the droplet. Ignoring its internal width the contact line is a three dimensional space curve $\mathscr{L}_{\alpha\beta\sigma}$ lying in the σ surface.

In a thermodynamic description, the free energy of the system can be written as a sum of free energies related to (i) the bulk phases, (ii) the interfaces between the bulk phases, and (iii) the contact line. A line energy Λ per length of the contact line can be introduced as an excess free energy with respect to the interfaces. The mechanical equilibrium condition of the contact line is expressed in terms of the generalized equation of Young–Dupré,

$$\Sigma_{\alpha\beta}\cos\theta = \Sigma_{\alpha\sigma} - \Sigma_{\beta\sigma} - c_{\mathrm{g}}^{*}\Lambda - \mathbf{m}\cdot\boldsymbol{\nabla}^{*}\Lambda \qquad \text{on } \mathscr{L}_{\alpha\beta\sigma}, \tag{2}$$

connecting the local contact angle θ to the interfacial tensions Σ_{ij} between phases i and j, the line tension Λ and the geometry of the contact line. In accordance with [8], we denote by c_{g}^{*} the geodesic curvature of the contact line with respect to the σ surface, the component of the total curvature of the contact line in the local tangential plane of the σ surface. The conormal vector $\mathbf{m}$ and the tangent of the contact line are orthonormal three dimensional vectors and form, together with the local surface normal to the σ surface, a right handed orthonormal frame in each point of the contact line. The covariant operator $\boldsymbol{\nabla}^{*}$ is the projection of the three dimensional nabla operator onto the local tangential plane of the σ surface.

The mechanical equilibrium condition (2) of the contact line which accounts for a non-zero line tension was first derived in its general form by Swain and Lipowsky in [15]; see also [1]. If both the σ surface is chemically homogeneous and the segment of the contact line under consideration is not curved the usual form of the equation of Young–Dupré, i.e., equation (2) without line tension terms, holds even in the presence of a non-zero line tension.

A small class of stationary configurations of the $\alpha\beta$ interface can be constructed analytically. In principle, one has to find a surface of constant mean curvature bounded by the σ surface and fulfilling the generalized form of the Young–Dupré equation (2). Since stationarity of a droplet does not necessarily imply its local stability, one has to consider the second variation of the free energy under general deformations of the $\alpha\beta$ interface. A detailed derivation of the second variation of the free energy for droplets on a smooth σ surface including spatially varying surface and line tensions is given in [8, 10]. The local stability of the droplet can be discussed in terms of the eigenvalue spectrum of the second variation: local stability is guaranteed if the smallest eigenvalue is positive. For stationary droplet shapes, the incompressibility condition of the wetting fluid β has to be taken into account only up to linear order which defines a subspace of volume conserving shape deformations.

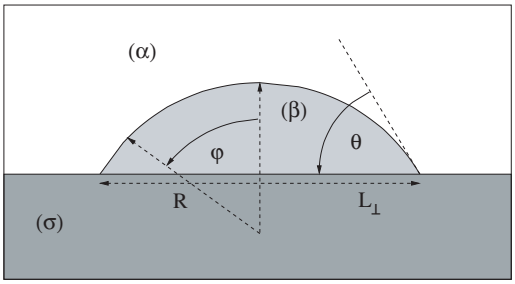

Figure 1. Cross section of a liquid channel on the homogeneous and planar substrate surface perpendicular to the z-axis. Greek symbols α, β, and σ denote the ambient fluid (vapour), the wetting liquid, and the rigid and inert substrate, respectively. The width $L_\perp$ of the stripe on σ wetted by β and the contact angle θ define the radius R of the cylinder segment. The azimuthal angle φ ranges from $-\theta$ to θ.

The eigenvalue spectrum of the second variation can be determined by solving Jacobi's accessory problem, a second order partial differential equation with linear boundary conditions. Dealing with an incompressible β fluid wetting the σ surface one has to restrict the set of solutions of this partial differential equation to a subset of solutions fulfilling the subsidiary condition of volume conservation up to a linear order. Details of the general stability analysis and the spectral stability criterion are described in [8, 10].

3. Cylindrical droplet geometry

On a planar and chemically homogeneous σ surface we may employ cylindrical surfaces as a special class of constant mean curvature surfaces to construct elementary droplet shapes. As schematically shown in figure 1, the $\alpha\beta$ interface of a liquid channel or filament is a cylindrical segment $\mathscr{A}_{\alpha\beta}$ obtained by one parallel and two perpendicular cuts with respect to the cylinder axis. In this particular case all terms in the generalized condition of Young–Dupré (2) containing the line tension drop out because the contact lines on either sides of the $\alpha\beta$ interface are straight lines.

The radius of the cylinder will be denoted by R and the length of the cut-out segment by $L_\parallel$. The width $L_\perp$ of the stripe on the σ surface in contact with the β liquid and the uniform contact angle θ of the cylinder segment determine the cylinder radius R via

$$R = \frac{L_\perp}{2\sin\theta}. \tag{3}$$

Using three dimensional Euclidean unit vectors $\mathbf{e}_\varphi$ and $\mathbf{e}_z$ which point into radial direction and along the axis of the cylinder, respectively, the surface $\mathscr{A}_{\alpha\beta}$ is parameterized in cylindrical coordinates by smooth functions $\mathbf{R}(\varphi, z) = \mathbf{e}_\varphi(\varphi)R + \mathbf{e}_z z$ with $-\theta \leqslant \varphi \leqslant \theta$ and $0 \leqslant z \leqslant L_\parallel$.

Following the general procedure of the stability analysis presented by us in [8], we have to solve the partial differential equation

$$-\left(\frac{1+\partial_\varphi^2}{R^2} + \partial_z^2 + \mu\right)\psi = \nu \tag{4}$$

on the cylindrical surface $\mathscr{A}_{\alpha\beta}$ with linear boundary conditions

$$\frac{\pm\partial_\varphi\psi}{R} - \frac{\cot\theta\,\psi}{R} - \frac{\Lambda\partial_z^2\psi}{\Sigma_{\alpha\beta}\sin^2\theta} = 0 \qquad \text{for } \varphi = \pm\theta, \tag{5}$$

where μ is the eigenvalue of the second variation and ν a Lagrangian parameter to ensure volume conservation up to the relevant order. Periodic boundary conditions are applied along the z-direction, i.e., parallel to the axis of the cylinder. Finally, the Lagrangian parameter ν has to be determined from the subsidiary condition of volume conservation up to linear order, which assumes the form

$$\int_{-\theta}^{\theta} \mathrm{d}\varphi \int_{0}^{L_\parallel} \mathrm{d}z\, \psi = 0 \tag{6}$$

for the particular case of a cylindrical segment $\mathscr{A}_{\alpha\beta}$.

The general solution ψ of the inhomogeneous partial differential equation (4) is a sum $\psi = \psi_\mathrm{h} + \psi_0$, where ψ_h belongs to the linear space of solutions to the homogeneous equation and ψ_0 is a particular solution to the corresponding inhomogeneous equation. For the moment, we will ignore the boundary conditions (5) and the periodicity along the channel and seek solutions ψ_0 of the inhomogeneous problem.

It turns out that, for the present case of a cylindrical channel, one may always find a particular inhomogeneous solution ψ_0 that is independent of z. For the general case $\mu \neq -1/R^2$, a particular solution of the inhomogeneous problem is

$$\psi_0 = -\frac{R^2\nu}{1 + R^2\mu}, \tag{7}$$

while in the exceptional case $\mu = -1/R^2$, a particular solution ψ_0 is provided by

$$\psi_0 = -\frac{\nu\varphi^2}{2}. \tag{8}$$

Since, in both cases, the solution ψ_0 to the inhomogeneous problem is periodic in the z-direction of the cylinder the homogeneous solution ψ is a linear combination

$$\psi_\mathrm{h} = \mathrm{e}^{\pm \mathrm{i}k_\parallel z}\big[A\cos(k_\perp\varphi) + B\sin(k_\perp\varphi)\big] \tag{9}$$

of periodic functions with yet unspecified arbitrary real numbers A and B. Because of the periodic boundary condition, the longitudinal wavenumbers

$$k_\parallel = 2\pi n/L_\parallel \tag{10}$$

are real with an integer longitudinal node number $n \geqslant 0$.

As the detailed analysis in the following sections will show, the boundary condition (5) allows a discrete set of transverse wavenumbers $k_\perp$ as solutions. We can conclude from equation (4) that the eigenvalues have the form

$$\mu = \frac{k_\perp^2 - 1}{R^2} + k_\parallel^2, \tag{11}$$

and, for later convenience, we define the 'transverse part'

$$\mu_\perp \equiv \frac{k_\perp^2 - 1}{R^2} = \frac{4\sin^2\theta(k_\perp^2 - 1)}{L_\perp^2} \tag{12}$$

of the eigenvalue μ. The only restriction on the transverse wavenumber $k_\perp$ is due to relation (11) since all eigenvalues μ of the second variation of the free energy have to be real numbers[4]. Therefore, a transverse wavenumber $k_\perp$ can be either a real or a purely imaginary complex number; compare equation (11).

Because the differential equation (4) and its boundary condition (5) remain unchanged upon replacing φ by $-\varphi$, the space of solutions ψ_h to the homogeneous equation can be

[4] The free energy is a real valued functional of the droplet configuration. Hence, we expect to find real coefficients in any order of an expansion in terms of a small parameter describing the shape deformation.

decomposed into the sum of two orthogonal linear subspaces containing solutions that are either *symmetric* (even) or *antisymmetric* (odd) in φ and, hence, $B = 0$ or $A = 0$ in the homogeneous solution (9), respectively.

Inspection of the linearized volume constraint (6) shows that we have $\nu = 0$ for (i) any homogeneous solution ψ_h with a node number $n > 0$ and (ii) any φ-odd homogeneous solution ψ_h independent of the longitudinal node number n. Only for φ-even solutions with $n = 0$ may we find $\nu \neq 0$. The φ-even solutions are given by

$$\psi_s = \begin{cases} A\left[\cos(k_\perp\varphi) - \dfrac{\sin(k_\perp\theta)}{k_\perp\theta}\right] & \text{for } n = 0 \\ A\mathrm{e}^{\pm \mathrm{i}k_\parallel z}\cos(k_\perp\varphi) & \text{for } n > 0, \end{cases} \tag{13}$$

while φ-odd solutions have the form

$$\psi_a = B\mathrm{e}^{\pm \mathrm{i}k_\parallel z}\sin(k_\perp\varphi) \qquad \text{for } n \geqslant 0. \tag{14}$$

When approaching $k_\perp = 0$, the φ-even solution (13) for $n > 0$ and the φ-odd solution (14) for $n \geqslant 0$ become $\psi_s = A\mathrm{e}^{\pm \mathrm{i}k_\parallel z}$ and $\psi_a = B\mathrm{e}^{\pm \mathrm{i}k_\parallel z}\varphi$, respectively. By inspection of equation (12) one can see that the exceptional case $-R^2\mu = 1$ is equivalent to $k_\perp = 0$ for φ-even $n = 0$ modes. Absorbing the factor $-k_\perp^2/2$ into the amplitude A, the φ-even $n = 0$ mode is given by $\psi_s = A(\varphi^2 - \theta^2/3)$. This can be seen by expanding the full solution (13) in terms of $k_\perp$ and keeping the leading order. One may also use an ansatz $\psi_h = A$ and the exceptional form (8) of the inhomogeneous solution ψ_0 which gives, after eliminating the parameter ν with the linearized volume constraint (6), the same result.

Solutions (13) and (14) fulfill the boundary condition (5) only for a discrete set of transverse wavenumbers $k_\perp$ and can be classified by the transverse node number m in addition to the longitudinal node number n. Through relation (12) the discrete set of transverse wavenumbers $k_\perp$ determines the transverse part $\mu_\perp$ of the eigenvalue μ. In the asymptotic stability analysis, $\mu < 0$ is a necessary condition for the occurrence of an instability. The definition (12) of $\mu_\perp$ shows that this condition can be fulfilled if the transverse wavenumber $k_\perp$ is (i) purely imaginary or (ii) a real number with $|k_\perp| < 1$, provided that $k_\parallel$ is sufficiently small. Therefore, the limit of local stability of the channel is obtained by solving the boundary condition (5) and the condition $\mu = 0$ *simultaneously*. This criterion is the basis of our stability analysis in the remainder of the paper.

In what follows, it is convenient to abbreviate the product of the contact angle θ and transverse wavenumber $k_\perp$ as

$$x \equiv k_\perp\theta. \tag{15}$$

By expressing any length in units of the channel width $L_\perp$ we define dimensionless eigenvalues $\bar{\mu} \equiv \mu L_\perp^2$ and $\bar{\mu}_\perp \equiv \mu_\perp L_\perp^2$, longitudinal wavenumbers $\bar{k}_\parallel \equiv k_\parallel L_\perp$ and wavelength $\bar{\lambda} \equiv \lambda/L_\perp = 2\pi/\bar{k}_\parallel$. In addition, it will be convenient to label the different deformation modes by the longitudinal node number n as defined in (10) and by the transversal node number m which follows from the solution of the discrete set of transverse wavenumbers $k_\perp$ or x as defined in (15).

4. Stability at zero line tension

We begin our stability analysis of liquid cylinders on chemically homogeneous and planar substrates with the case of a vanishing line tension $\Lambda = 0$. This situation has already been considered in [12] and [13]. We recover these previous results and extend them in the following section 5 by considering the influence of positive or negative contact line tension.

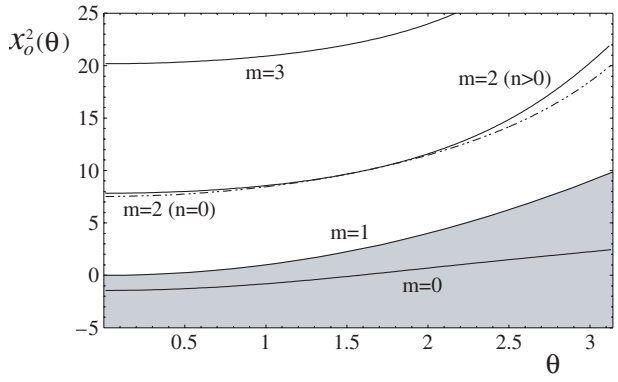

Figure 2. Branches of x_o^2 as a function of the contact angle θ at zero line tension $\Lambda = 0$. Solutions to equations (17) and (18) are shown as solid curves while solutions to equation (19) are displayed as dashed curves. All solutions $x = x_o(\theta)$ are monotonically increasing functions of the contact angle θ. Shown are the first φ-even (even m) and φ-odd modes (odd m). According to equation (11), negative eigenvalues μ are encountered in the grey shaded region where $x_o^2 < \theta^2$. Channel instabilities may occur only for modes with transversal node numbers $m = 0$ and longitudinal node numbers $n > 0$ at a sufficiently small $\bar{k}_\parallel$. The first φ-odd mode with $(m, n) = (1, 0)$ coincides with the marginal case $x_o^2 = \theta^2$.

Inspection of boundary condition (5) shows that the transverse part $\mu_\perp$ of the eigenvalue μ of the second variation does not depend on the wavenumber $k_\parallel$ for $\Lambda = 0$. After inserting the modes (13) and (14) into the boundary condition (5) we are able to compute solution branches $x = x_o(\theta)$ of the transverse wavenumber and their square $x_o^2(\theta)$ for (i) φ-even modes ψ_s with longitudinal node numbers $n = 0$, (ii) φ-odd modes ψ_a with $n \geqslant 0$, and (iii) φ-even modes ψ_s with $n > 0$. According to equations (11) and (12) the channel may become unstable whenever $\mu_\perp < 0$ or equivalently $x_o^2(\theta) < \theta^2$ with respect to perturbations with rescaled longitudinal wavelengths $\bar{\lambda}$ *larger* than

$$\bar{\lambda}_{\max}(\theta) = \frac{2\pi}{\sqrt{-\mu_\perp}} = \frac{\pi}{\sin\theta}\sqrt{\frac{\theta^2}{\theta^2 - x_o^2(\theta)}}. \tag{16}$$

Figure 2 shows the smallest branches $x_o^2(\theta)$ for both φ-even and φ-odd modes.

4.1. Symmetric (φ-even) modes with $n = 0$

After inserting the generic form (13) of the φ-even eigenfunction ψ_s with $n = 0$ into the boundary condition (5) for vanishing line tension $\Lambda = 0$ we arrive at an equation

$$x \tan x + \theta \cot\theta \left(1 - \frac{\tan x}{x}\right) = 0 \tag{17}$$

in the rescaled transverse wavevector x. Since the generic form (13) of the φ-even eigenfunction ψ_s and, hence, equation (17) is valid only for $k_\perp \neq 0$, we have to consider the exceptional case $x = 0$ separately. One can easily check that the exceptional form of the φ-even mode $\psi_s = A(\varphi^2 - \theta^2/3)$ cannot fulfill the boundary condition (5) for any non-zero contact angle $\theta \leqslant \pi$.

Equation (17) has a discrete set of solution branches $x = x_o(\theta)$. The eigenfunction ψ_s belonging to the solution branch $x_o(\theta)$ of equation (17) which yields the smallest values $x^2 = x_o^2(\theta)$ and thus the smallest value of $\mu_\perp$ exhibits two transverse nodes, i.e., has a transverse node number $m = 2$. Solution branches $x_o(\theta)$ of (17) are symmetrically distributed around

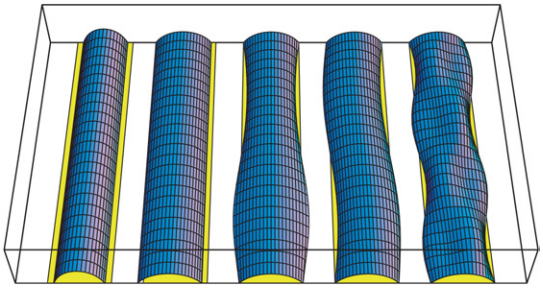

Figure 3. Deformation eigenmodes of the liquid–vapour interface with transverse and longitudinal node number m and n, respectively, bounding a cylindrical segment. Displayed are (from left to right) the lowest z-independent $(m, n) = (2, 0)$ mode, the transverse shift mode $(1, 0)$, the lowest varicose $(0, 1)$ mode, the lowest zig-zag $(1, 1)$ mode, and a higher φ-odd mode $(3, 2)$. The area of the substrate surface in contact with the liquid prior to deformation corresponds to the light grey (yellow) stripe. For all deformation modes, the volume of the liquid channel is conserved in a linear order.

$x = 0$ and have been systematically studied by numerical methods. No purely imaginary values of $x = x_o(\theta)$ are encountered at any contact angle $0 \leqslant \theta \leqslant \pi$. In particular, we find values $x_o(0) \simeq 2.74$, $x_o(\pi/2) = \pi$, and $x_o(\pi) \simeq 4.49$. Figure 2 shows the branch $x_o^2(\theta)$ corresponding to a deformation mode with node numbers $(m, n) = (2, 0)$ as a function of θ, confirming that $x_o^2(\theta) > \theta^2$ for all contact angles and, hence, the $(2, 0)$ mode does not destabilize the channel. The latter mode will be called the bouncing mode since it corresponds to deformation in which the liquid channel filament 'bounces' back and forth between a weakly and a strongly adsorbed state; see figure 3.

The fact that no instability is caused by $n = 0$ modes can be already understood by considering all stationary solutions which are invariant under translations into the z-direction. This class of constant mean curvature surfaces comprises only cylindrical channels because segments of a circle are the only contour lines bearing a constant curvature. At a given length $L_\parallel$ and width $L_\perp$ of a channel, we may use the contact angle θ to parameterize the branch of stationary channel configurations. By simple geometry one can show that the channel volume V is a strictly monotonically increasing function in θ.

Furthermore, we can suppress the soft translation mode of the channel configurations perpendicular to the z-direction since it is a soft translation mode for all configurations. Then, the local stability can only change at a bifurcation point or at a fold where a volume conserving linear subspace of stationary solutions exists. This subspace is spanned by modes with zero eigenvalue which exhibit the *same symmetry* as the stationary configurations. Since this is not the case here we conclude that all eigenvalues μ corresponding to volume conserving $n = 0$ deformation modes cannot become zero. According to our analysis we have $\mu > 0$ for all branches of eigenvalues corresponding to the $n = 0$ deformation modes (except for the soft translation mode perpendicular to the channel).

4.2. Antisymmetric (φ-odd) modes with $n \geqslant 0$

The boundary condition for φ-odd solutions ψ_a with longitudinal node number $n \geqslant 0$ becomes

$$x \cot x - \theta \cot \theta = 0 \tag{18}$$

in the case $\Lambda = 0$, which is solved by $x = x_o(\theta) = \theta$, and, hence, $k_\perp = 1$ for the $m = 1$ mode independent of the value of the contact angle θ. This solution branch corresponds to a soft mode with node numbers $(m, n) = (1, 0)$ with $\bar{\mu} = 0$ since we have $\bar{k}_\parallel = 0$ (which implies

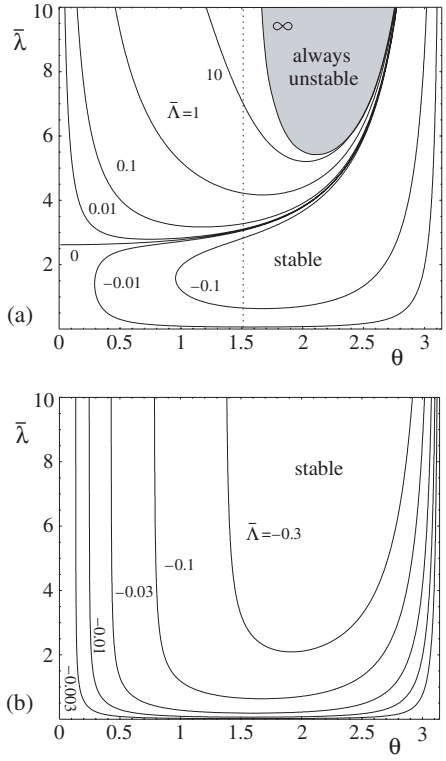

Figure 4. Stability diagram of a liquid channel on a homogeneous and planar substrate for different values of the dimensionless line tension $\bar{\Lambda} = \Lambda/\Sigma_{\alpha\beta}L_\perp$. The cylindrical liquid–vapour interface of the channel with contact angle θ is exposed (a) to the symmetric varicose mode with $(m, n) = (0, 1)$ and (b) to the asymmetric zig-zag mode with $(m, n) = (1, 1)$; compare figure 3. The longitudinal wavelength of deformations is $\bar{\lambda} = \lambda/L_\perp = 2\pi/k_\parallel L_\perp$. Both in (a) and (b), the stable region forms a 'tongue' for negative values of the line tension $\bar{\Lambda}$. The smallest 'tongues' displayed in (a) and (b) correspond to $\bar{\Lambda} = -0.1$ and $\bar{\Lambda} = -0.3$, respectively. These 'tongues' grow with increasing $\bar{\Lambda}$. In the limit of large $\bar{\Lambda}$, the 'tongue' covers the whole $(\theta, \bar{\Lambda})$-plane in (b) but leaves the grey region uncovered in (a). The latter region corresponds to a liquid channel or filament with pinned contact lines and approaches the dashed line $\theta = \pi/2$.

$\bar{\mu}_\parallel = 0$) and $\bar{\mu}_\perp = 0$, while $x_o^2(\theta)$ coincides with the boundary of the stable region displayed in figure 2. However, the channel is stable with respect to all $(1, n)$ modes with $n > 0$ where an inequality $\bar{\mu}_\perp > 0$ holds.

The $(1, 0)$ mode with $k_\perp = 1$ describes a transverse shift of the entire channel morphology; see figure 3. This soft deformation mode is a direct consequence of the continuous translational symmetry in the direction perpendicular to the channel. For higher longitudinal node numbers $n > 0$, the related φ-odd solutions describe a zig-zag-like deformation of the cylindrical segment; compare figure 3. The asymptotic results for the next larger solution branch $x = x_o(\theta)$ of equation (18) corresponds to a mode with a transverse node number $m = 3$ and assumes values $x_o(0) \simeq 4.49, x_o(\pi/2) = 3\pi/2$, and $x_o(\pi) = 2\pi$. The corresponding shape of the $(3, 2)$ mode is shown in figure 3. In general, we have $x_o(\pi/2) = \pi m/2$ and $x_o(\pi) = \pi(m + 1)/2$.

4.3. Symmetric (φ-even) modes with $n > 0$

All φ-even modes ψ_s with $n > 0$ in the case $\Lambda = 0$ have to satisfy the boundary condition

$$x \tan x + \theta \cot \theta = 0. \tag{19}$$

In agreement with the results of [12] we find a solution branch $x = x_o(\theta)$ with the particular value $x_o(0) = \mathrm{i}y_o$ where $y_o \simeq 1.12$. The numerical value of y_o is given by the smallest solution y to the equation $y \tanh y = 1$. The φ-even mode ψ_s that corresponds to this root yields the smallest values $x^2 = x_o^2(\theta)$ for any contact angle $0 \leqslant \theta \leqslant \pi$, has no transverse nodes and thus a node number $m = 0$.

According to equation (16) liquid channels are unstable with respect to the (0, 1) mode for small values of θ whenever the rescaled longitudinal wavelength of the perturbation is larger than the value of

$$\bar{\lambda}_{\max}(0) = \frac{\pi}{y_o} \simeq 2.62, \tag{20}$$

which applies to a sufficiently long channel with $L_\parallel > \lambda_{\max}(0)$. This destabilizing mode exhibits a varicose shape as shown in figure 3.

The rescaled transverse wavenumber of the (0, 1) mode given by the solution branch $x = x_o(\theta)$ stays purely imaginary for all contact angles $\theta < \pi/2$. We have $x_o(\pi/2) = 0$, while $x_o(\theta)$ becomes a positive, real number for $\theta > \pi/2$ that increases monotonically with θ. We find $x_o(\pi) = \pi/2$ and thus the asymptotic form $\bar{\mu}_\perp \approx -3(\pi - \theta)^2$. Therefore, $x_o^2(\theta) < \theta^2$ for all possible values of θ and, hence, we find $\mu_\perp < 0$ for any contact angle $0 \leqslant \theta \leqslant \pi$. The corresponding instability with respect to φ-odd $(0, n)$ modes occurs for channel lengths $\bar{L}_\parallel > \bar{\lambda}_{\max}(\theta)$, where $\bar{\lambda}_{\max}(\theta)$ is given by equation (16) and depends on the contact angle θ. The numerical result for the function $\bar{\lambda}_{\max}(\theta)$ is shown in figure 4(a). In the limit of small θ, it approaches $\bar{\lambda}_{\max}(0) \simeq 2.62$, while, according to equation (16), $x_o(\pi) = \pi/2$ causes the asymptotic behaviour

$$\bar{\lambda}_{\max}(\theta) \approx \frac{2\pi}{\sqrt{3}(\pi - \theta)}. \tag{21}$$

The next solution branch $x = x_o(\theta)$ of equation (19) corresponding to φ-even modes with (even) $m \geqslant 2$ is found to be real and to satisfy $k_\perp^2 > 1$; that is, φ-even $m \geqslant 2$ modes do not cause instabilities. This can be seen by considering asymptotic results for the solution branch $x_o(\theta)$ fulfilling (19) for $m = 2$ with values $x_o(0) \simeq 2.80$, $x_o(\pi/2) = \pi$, and $x_o(\pi) = 3\pi/2$. The branch of solutions satisfies $x_o^2(\theta) > \theta^2$ and no instability is caused; cf figure 2. As for the case of symmetric modes, we find the solutions to satisfy $x_o(\pi/2) = \pi m/2$ and $x_o(\pi) = \pi(m + 1)/2$.

In the context of surface melting, McCallum *et al* considered the stability of a solid cylindrical channel by applying a diffusive interface dynamics which yields the same result for the 'neutral stability' boundaries [16]. Although in [16] a different method is used to describe the shape of the channel, the results agree for the particular case considered here. This is not surprising since McCallum *et al* use isotropic interfacial energies and an interface dynamics with conserved order parameter equivalent to the volume constraint (6).

5. Effect of line tension

Inspection of the general form of the boundary conditions (5) shows that the conditions (18) and (19) have to be modified for a non-zero contact line tension $\Lambda \neq 0$. Condition (17) applies only to φ-odd modes with $n = 0$; that is, with a longitudinal wavenumber $k_\parallel = 0$. The length of the contact line does not change under a deformation mode with $n = 0$, and, hence, the line tension does not affect the eigenvalue spectrum of these modes. In the following, it will be convenient to use the dimensionless line tension

$$\bar{\Lambda} \equiv \Lambda/(\Sigma_{\alpha\beta} L_\perp). \tag{22}$$

Insertion of φ-even modes ψ_s with $n \geqslant 0$ into the full boundary condition (5) we arrive at the condition

$$x \tan x + \theta \left(\cot\theta - \frac{\bar{\Lambda}\bar{k}_\parallel^2}{2\sin^3\theta} \right) = 0 \tag{23}$$

while for φ-odd modes ψ_a with $n \geqslant 0$ equation (5) becomes

$$x \cot x - \theta \left(\cot\theta - \frac{\bar{\Lambda}\bar{k}_\parallel^2}{2\sin^3\theta} \right) = 0. \tag{24}$$

Both conditions (23) and (24) lead to a solution of the form

$$\bar{\Lambda} = \bar{\Lambda}_j(x, \theta, \bar{k}_\parallel) \qquad \text{for } j = s, a \tag{25}$$

with $x = k_\perp \theta$ as before and $j = s, a$ for φ-even and φ-odd modes, respectively. Both conditions depend on the rescaled longitudinal wavenumber $\bar{k}_\parallel = k_\parallel L_\perp$ in contrast to conditions (18) and (19) for vanishing line tension, which are independent of $\bar{k}_\parallel$. Hence, the transverse part $\mu_\perp$ of the rescaled eigenvalue $\bar{\mu}$ becomes implicitly dependent on $\bar{k}_\parallel$. According to (11) and (12) we can rephrase the condition $\bar{\mu} = 0$ for a channel at the stability limit as

$$\bar{\mu} = 4\sin^2\theta \left(\frac{x^2}{\theta^2} - 1 \right) + \bar{k}_\parallel^2 = 0 \tag{26}$$

which can be solved in terms of a function $x = x_o(\theta, k_\parallel)$. Equation (26) along with equation (23) or (24) determines the limit of stability. Upon inserting the function $x = x_o(\theta, k_\parallel)$ into expression (25), we obtain a new function

$$\bar{\Lambda} = \bar{\Lambda}_j\big(x_o(\theta, \bar{k}_\parallel), \theta, \bar{k}_\parallel\big) \equiv \bar{\Lambda}_{o,j}(\theta, \bar{k}_\parallel) \tag{27}$$

for $j = s, a$. This function gives the value of the line tension $\bar{\Lambda}$ of a channel with contact angle θ on the boundary of local stability with respect to a deformation mode with longitudinal wavenumber $\bar{k}_\parallel$ and symmetry j.

On the one hand, one can prove that the square x^2 of a solution $x = x_o$ to equation (23) or (24) at fixed θ and $k_\parallel$ is monotonically increasing with increasing line tension $\bar{\Lambda}$. The definition (12) of the transverse part $\mu_\perp$ of the eigenvalue $\bar{\mu}$ and the definition (11) of the eigenvalue shows, on the other hand, that $\bar{\mu}$ is monotonically increasing with an increasing value of x^2. Hence, the solution $\bar{\Lambda} = \bar{\Lambda}_{o,j}(\theta, \bar{k}_\parallel)$ is the *smallest value* of the line tension where a liquid channel or filament is stable for given values of the contact angle θ and the longitudinal wavenumber $\bar{k}_\parallel$ or wavelength $\bar{\lambda} = 2\pi/\bar{k}_\parallel$.

This procedure can be easily implemented numerically and the results are presented in the form of a stability diagram in the $(\theta, \bar{\lambda})$ plane in figures 4(a) and (b) for the φ-odd (0, 1) mode and the φ-even (1, 1) mode, respectively. Both diagrams in figure 4 can be interpreted in two ways: either the lines can be seen as lines of equal $\bar{\Lambda}_{o,j}$, and the channel with contact angle θ is unstable with respect to a mode with given wavelength $\bar{\lambda}$ whenever we have $\bar{\Lambda} < \bar{\Lambda}_{o,j}$; or we interpret the lines as boundaries $(\theta, \bar{\lambda})$ limiting the region of stability for given line tension $\bar{\Lambda}$ and contact angle θ. The region of stable channels is always located on the side where lower values of $\bar{\Lambda}_{o,j}$ are indicated.

5.1. Positive line tension

It is intuitively clear that a positive line tension tends to stabilize a liquid channel or filament. In the limit of large $\bar{\Lambda}$, the stability boundary of the channel with line tension should approach the stability boundary of a liquid channel with a fixed or *pinned* contact line, a problem which

has been considered previously in [3, 13]. In the limit of infinite $\bar{\Lambda}$, we find $x_o = \pi/2$ as the solution belonging to the smallest value for $\mu_\perp$, and the condition $\mu = 0$ becomes

$$\bar{\lambda}_{\max}(\theta) = \frac{\pi}{\sin\theta}\sqrt{\frac{\theta^2}{\theta^2 - \pi^2/4}}, \tag{28}$$

as obtained previously in [3, 13] for a pinned contact line. Equation (28) for the stability boundary of modes with $m = 0$ defines the grey region $\bar{\lambda} > \bar{\lambda}_{\max}(\theta)$ in figure 4(a). The channel is *always* unstable with respect to $m = 0$ modes inside the grey region irrespective of the magnitude of $\bar{\Lambda}$.

Note that the spectrum of deformation modes with $n = 0$, including the $(1, 0)$ mode related to the translation perpendicular to the z-direction, is different from the case of a pinned contact line even in the limit of large positive line tension $\bar{\Lambda}$. In contrast to a channel on a chemically homogeneous and planar substrate, a pinned channel cannot move as a whole into the direction perpendicular to the z-axis. Contact line pinning may be achieved by a chemical stripe with enhanced wettability [3] or by surface topographies such as the upper edges of a rectangular groove [17].

5.2. Negative line tension

If the line tension is decreased to negative values, the stability region with respect to the lowest varicose mode with $(m, n) = (0, 1)$, compare figure 3, shrinks and attains the shape of a 'tongue' as displayed in figure 4(a). Inspection of this latter figure shows that the stability region is bounded from above by the stability line corresponding to $\bar{\lambda} = \bar{\lambda}_{\max}(\theta)$ for vanishing line tension $\bar{\Lambda} = 0$. This latter line is special since it forms a right angle with the $\bar{\lambda}$-axis; see figure 4(a). In addition, the stability 'tongue' for negative line tension is bounded by instability regions at small contact angle, short wavelength and large contact angle. In this subsection, we will address the unstable modes which are present at short wavelengths; in the next subsection, we will discuss those at small contact angle.

In order to study the instabilities with respect to short wavelength deformations, we consider the limit of large $k_\parallel$ in (26) which leads to an approximate function

$$x_o(\theta, \bar{k}_\parallel) \approx \pm\frac{\mathrm{i}\bar{k}_\parallel\theta}{2\sin\theta}. \tag{29}$$

On inserting expression (29) into equation (23) or (24) for φ-even or φ-odd modes, respectively, and taking the limit of large $k_\parallel$, one attains the approximate condition

$$\frac{\bar{k}_\parallel\theta}{2\sin\theta} - \theta\cot\theta + \frac{\bar{\Lambda}\bar{k}_\parallel^2\theta}{2\sin^3\theta} \approx 0 \tag{30}$$

for the stability boundary, which implies that $\bar{k}_\parallel \approx \sin^2\theta/|\bar{\Lambda}|$ unless θ is small. Thus, the stability 'tongue' is bounded from below by the minimal wavelength

$$\bar{\lambda}_{\min}(\theta) \approx \frac{2\pi|\bar{\Lambda}|}{\sin^2\theta} \qquad \text{or} \qquad \lambda_{\min}(\theta) \approx \frac{2\pi}{\sin^2\theta}\frac{|\Lambda|}{\Sigma_{\alpha\beta}} \equiv \frac{2\pi}{\sin^2\theta}L_\beta^*, \tag{31}$$

for small $|\bar{\Lambda}|$ for both φ-even and φ-odd modes; see figures 4(a) and (b), respectively. The characteristic wavelength $L_\beta^* = |\Lambda|/\Sigma_{\alpha\beta}$ represents the linear size of a wetting morphology for which the contact line free energy is comparable to the interfacial free energy [1].

As shown in figure 4(a), the stable region in the $(\theta, \bar{\lambda})$ plane forms a 'tongue', the shape of which depends on the line tension $\bar{\Lambda}$. As long as $\bar{\Lambda} < 0$, the stability 'tongue' does not touch any boundary of the $(\theta, \bar{\lambda})$ plane. As one approaches the limiting value $\bar{\Lambda} = 0$ from

below, this stability 'tongue' evolves in a singular manner. Indeed, in this limit, the 'tongue' grows continuously and approaches the three boundaries as given by (i) $\theta = \pi$, (ii) $\bar{\lambda} = 0$, and (iii) $\theta = 0$ with $\bar{\lambda} < \bar{\lambda}_{\max}(0) \simeq 2.62$; see figure 4(a). This singular behaviour is related to the fact that the line tension term in the boundary condition (5) represents a singular perturbation since the line tension Λ multiplies the highest derivative which occurs in this equation.

In the continuum model considered here, the estimate (31) implies the instability of *all* deformation modes with wavelengths $0 < \lambda < 2\pi L_\beta^*$ irrespective of the value of the contact angle θ. However, deformation modes with arbitrarily short wavenumbers cannot occur in real systems which are characterized by additional microscopic length scales. The largest of these latter scales should be provided by the intrinsic width $\ell_{\alpha\beta\sigma}$ of the contact line [1]. Clearly, the continuum description of the deformation modes breaks down as soon as their wavenumber λ becomes comparable to $\ell_{\alpha\beta\sigma}$. Therefore, one should exclude the region

$$\bar{\lambda} \lesssim \bar{\ell}_{\alpha\beta\sigma} \equiv \ell_{\alpha\beta\sigma}/L_\perp \tag{32}$$

from the stability diagrams in figures 4(a) and (b).

It is instructive to use dimensional analysis in order to get some rough estimates of the various quantities involved [1]. Thus, let us take the temperature T as the basic energy scale (where the symbol T represents the Boltzmann constant times the temperature in kelvins) and the molecular size ℓ_{mol} as the basic length scale. In the liquid state, the free energy per unit volume is of the order of T/ℓ_{mol}^3. We can then express the interfacial tension $\Sigma_{\alpha\beta}$ and the line tension Λ as

$$\Sigma_{\alpha\beta} = c_\Sigma (T/\ell_{\mathrm{mol}}^3)\ell_{\mathrm{mol}} \qquad \text{and} \qquad |\Lambda| = c_\Lambda^2 (T/\ell_{\mathrm{mol}}^3)\ell_{\mathrm{mol}}^2 \tag{33}$$

with dimensionless coefficients c_Σ and c_Λ which are presumably nonuniversal, i.e., depend on the molecular composition and the molecular interactions. On the other hand, we may also *define* the intrinsic width $\ell_{\alpha\beta}$ of the liquid–vapour interface and the intrinsic width $\ell_{\alpha\beta\sigma}$ of the three phase contact line by

$$\Sigma_{\alpha\beta} \equiv (T/\ell_{\mathrm{mol}}^3)\ell_{\alpha\beta} \qquad \text{and} \qquad |\Lambda| = (T/\ell_{\mathrm{mol}}^3)\ell_{\alpha\beta\sigma}^2 \tag{34}$$

which implies

$$\ell_{\alpha\beta} = c_\Sigma \ell_{\mathrm{mol}} \qquad \text{and} \qquad \ell_{\alpha\beta\sigma} = c_\Lambda \ell_{\mathrm{mol}}. \tag{35}$$

Using these relations, the crossover length $L_\beta^* = |\Lambda|/\Sigma_{\alpha\beta}$ can now be expressed as

$$L_\beta^* = (c_\Lambda^2/c_\Sigma)\ell_{\mathrm{mol}} = \ell_{\alpha\beta\sigma}^2/\ell_{\alpha\beta}, \tag{36}$$

and the short wavelength band $\ell_{\alpha\beta\sigma} < \lambda < L_\beta^*$ of unstable deformation modes now becomes

$$c_\Lambda < \frac{\lambda}{\ell_{\mathrm{mol}}} < \frac{c_\Lambda^2}{c_\Sigma} \qquad \text{or} \qquad \frac{c_\Sigma}{c_\Lambda} < \frac{\lambda}{L_\beta^*} < 1. \tag{37}$$

As long as one stays away from a critical point of the liquid or liquid mixture, the experimental values for the interfacial tensions imply that the dimensionless coefficient c_Σ is of the order of one. In contrast, the experimentally determined values for the line tension cover the relatively wide range $1 \lesssim c_\Lambda \lesssim 300$ [1]. Using these estimates in the inequalities (37), one concludes that the short wavelength band of unstable modes is presumably *absent* for $c_\Lambda \simeq 1$. In contrast, for $c_\Lambda \simeq 100$, such a band should be present and given by $1 < \lambda/\ell_{\mathrm{mol}} < 10^4$ or $10^{-2} < \lambda/L_\beta^* < 1$.

Thus, for $c_\Lambda \gg 1$, one should have a short wavelength band of unstable modes even if one includes the short wavelength cutoff provided by the molecular length scales. The estimate $1/c_\Lambda \lesssim \lambda/L_\beta^* < 1$ then indicates that these unstable modes lead to new liquid morphologies which exhibit undulations with a wavelength of the order of L_β^*. It would be interesting to test this prediction by computer simulations.

5.3. Small contact angle

Inspection of figure 4(a) shows that the stability of the liquid channel or filament for small values of the contact angle θ depends strongly on the sign of the line tension $\bar{\Lambda}$. For $\bar{\Lambda} < 0$, one has a stability 'tongue' which is bounded from the left by $\theta = \theta_{\min}(\bar{\Lambda})$. For $\bar{\Lambda} \geqslant 0$, the stability region is bounded from above by $\lambda = \lambda_{\max}(\theta)$. For small θ, the latter function attains the finite limit $\lambda_{\max}(0) \simeq 2.62$ for $\bar{\Lambda} = 0$, see equation (20), but grows as $\lambda_{\max}(\theta) \propto 1/\theta$ for $\bar{\Lambda} > 0$. This behaviour will now be derived from the boundary conditions for the case of φ-even deformation modes.

As a starting point, we replace the boundary condition (26) by the simplified approximate function

$$x_o(\theta, \bar{k}_\parallel) \approx \pm \frac{\mathrm{i}\bar{k}_\parallel}{2}, \tag{38}$$

valid for a liquid channel or filament on the limit of stability for small contact angles $\theta \ll 1$. Inserting the approximation (38) into equation (23) leads us to an approximate condition

$$\frac{\bar{k}_\parallel}{2} \tanh\left(\frac{\bar{k}_\parallel}{2}\right) - 1 + \frac{\bar{\Lambda}\bar{k}_\parallel^2}{2\theta^2} \approx 0. \tag{39}$$

Solutions $\bar{k}_\parallel$ to equation (39) become small for large, positive values of the line tension $\bar{\Lambda} \gg \theta^2$ and we can safely neglect the first term in equation (39). One obtains $\bar{k}_\parallel = \sqrt{2\theta^2/\bar{\Lambda}}$ and the asymptotic scaling

$$\bar{\lambda}_{\max}(\theta) \approx \frac{\pi\sqrt{2\bar{\Lambda}}}{\theta} \tag{40}$$

for the largest stable longitudinal wavelength. The diverging stability boundary $\bar{\lambda}_{\max} \propto 1/\theta$ for small θ can be clearly seen in figure 4(a). For zero line tension $\bar{\Lambda} = 0$ in equation (39), we recover the solution $\bar{k}_\parallel = y_o/2$ of the $m = 0$ mode discussed previously.

For negative values of the line tension $\bar{\Lambda} = -|\bar{\Lambda}|$, we find a minimal contact angle

$$\theta_{\min} \approx c_{\min}\sqrt{|\bar{\Lambda}|} \tag{41}$$

for small $|\Lambda|$ with a dimensionless coefficient $c_{\min}$ such that there is no solution to equation (39) for the contact angle range $\theta < \theta_{\min}$. When θ exceeds $\theta_{\min}$, two solutions $\bar{k}_\parallel^{\max}$ and $\bar{k}_\parallel^{\min}$ emerge with $\bar{k}_\parallel^{\max} > \bar{k}_\parallel^{\min}$. From our numerical investigation, we obtain the estimate

$$c_{\min} \simeq 2.90. \tag{42}$$

For $\theta = \theta_{\min} \approx c_{\min}\sqrt{|\bar{\Lambda}|}$, equation (39) has exactly one solution $\bar{k}_\parallel^{\max} = \bar{k}_\parallel^{\min} \simeq 4.53$. For $\theta > \theta_{\min}$, this equation has two solutions $\bar{\lambda}_{\min} = 2\pi/\bar{k}_\parallel^{\max}$ and $\bar{\lambda}_{\max} = 2\pi/\bar{k}_\parallel^{\min}$ which define the stability 'tongue'. This 'tongue' terminates at the minimum contact angle $\theta = \theta_{\min}$ and at the wavelength $\bar{\lambda}_{\min}(\theta_{\min}) = \bar{\lambda}_{\max}(\theta_{\min}) \simeq 1.39$ (which is roughly half of the value for $\bar{\lambda}_{\max}(0) \simeq 2.62$ for $\bar{\Lambda} = 0$).

6. Conclusion

We have performed a stability analysis for cylindrical liquid channels or filaments on planar and chemically homogeneous substrates. Our main result is the complete stability diagram as a function of the contact angle θ, the reduced longitudinal wavelength $\bar{\lambda} = \lambda/L_\perp$ and the reduced line tension $\bar{\Lambda} = \Lambda/\Sigma_{\alpha\beta}L_\perp$ as displayed in figure 4. As one reaches the boundaries of the stable regions, the channel or filament undergoes a Rayleigh–Plateau-like instability.

We find that a positive line tension $\Lambda > 0$ stabilizes the cylindrical channel morphology beyond the maximal wavelength for zero line tension. In fact, the line tension Λ enters the boundary condition (5) only in the form $\Lambda/\sin^2\theta$ which can be regarded as an effective, θ-dependent line tension. Therefore, stabilization by a positive line tension is particularly strong for small contact angle θ and, thus, large effective line tension $\Lambda/\sin^2\theta$. This leads to a maximal stable wavelength $\lambda_{\max}$ which increases as $\lambda_{\max} \sim 1/\theta$ for small contact angles θ as follows from (40).

As one decreases the line tension towards negative values $\Lambda < 0$, the stability region with respect to the lowest varicose mode shrinks and attains the form of a 'tongue'; see figure 4(a). This 'tongue' is bounded by several unstable regions. First, the liquid channel or filament becomes again unstable with respect to long wavelength perturbations as in the case of positive line tension. In addition, the continuum theory considered here predicts a band of unstable short wavelength modes. We have argued that the presence or absence of this band depends on the dimensionless coefficient c_Λ which is defined in (33) and which is equal to the ratio of contact line width to molecular size. A band of unstable short wavelength deformations should be absent and present if $c_\Lambda \simeq 1$ and $c_\Lambda \gg 1$, respectively. If they are present, these unstable modes presumably lead to liquid structures which exhibit some short wavelength waviness or undulations. In addition, no stability region exists for negative line tension and sufficiently small contact angles $\theta < \theta_{\min}$ with $\theta_{\min} \approx c_{\min}\sqrt{|\bar{\Lambda}|}$ and $c_{\min} \simeq 2.90$ for small negative line tension Λ as given by (41) and (42). In the latter case, liquid channels or filaments would have a very short lifetime before they decay into different morphologies.

Very recently, Rosso and Virga [18] also performed a stability analysis of liquid channels or filaments (which they call liquid bridges) taking into account the effects of line tension. Using rather different calculational methods, they conclude that these morphologies exhibit a certain regime of stability even for negative line tension, which agrees with our results.

Acknowledgments

We thank the referees for drawing our attention to [18] and for their detailed comments on our manuscript.

References

[1] Lipowsky R, Lenz P and Swain P S 2000 *Colloids Surf.* A **161** 3
[2] Pompe T, Fery A and Herminghaus S 1999 *J. Adhes. Sci. Technol.* **13** 1155
[3] Gau H, Herminghaus S, Lenz P and Lipowsky R 1999 *Science* **283** 46
[4] Brinkmann M and Lipowsky R 2002 *J. Appl. Phys.* **92** 4296
[5] Kubalski G P and Napiórkowski M 2000 *J. Phys.: Condens. Matter* **12** 9221
[6] Rowlinson J S and Widom B 1982 *Molecular Theory of Capillarity* (Oxford: Clarendon)
[7] Indekeu J O 1994 *Int. J. Mod. Phys.* B **8** 309
[8] Brinkmann M, Kierfeld J and Lipowsky R 2004 *J. Phys. A: Math. Gen.* **37** 11547
[9] Rosso R and Virga E G 2003 *Phys. Rev.* E **68** 012601
[10] Rosso R and Virga E G 2004 *J. Phys. A: Math. Gen.* **37** 3989
[11] Lord Rayleigh 1879 *Proc. R. Soc.* **29** 71
[12] Sekimoto K, Oguma R and Kawazaki K 1987 *Ann. Phys.* **176** 359
[13] Lenz P and Lipowsky R 2000 *Eur. Phys. J.* E **1** 249
[14] do Carmo M 1976 *Differential Geometry of Curves and Surfaces* (Englewood Cliffs, NJ: Prentice Hall)
[15] Swain P S and Lipowsky R 1998 *Langmuir* **14** 6772
[16] McCallum M S, Voorhees P W, Miksis M J, Davis S H and Wong H 1996 *J. Appl. Phys.* **79** 7604
[17] Seemann R, Brinkmann M, Kramer E, Lange F F and Lipowsky 2005 *Proc. Natl Acad. Sci. USA* **102** 1848
[18] Rosso R and Virga E G 2004 *Phys. Rev.* E **70** 031603